Biosensors and Bioelectronics 64 (2015) 102–110

Contents lists available at ScienceDirect

Biosensors and Bioelectronics

journal homepage: www.elsevier.com/locate/bios

Integrated catheter system for continuous glucose measurement and simultaneous insulin infusion

Barbara Nacht [a], Christoph Larndorfer [a], Stefan Sax [b], Sergey M. Borisov [a], Martin Hajnsek [c], Frank Sinner [c], Emil J.W. List-Kratochvil [b,d], Ingo Klimant [a,*]

[a] Institute of Analytical Chemistry and Food Chemistry, Graz University of Technology, Stremayrgasse 9/II, Graz 8010, Austria
[b] NanoTecCenter Weiz Forschungsgesellschaft mbH, Franz-Pichler-Straße 32, Weiz 8160, Austria
[c] Joanneum Research GmbH, Elisabethstraße 5, Graz 8010, Austria
[d] Institute of Solid State Physics, Graz University of Technology, Petersgasse 16, Graz 8010, Austria

ARTICLE INFO

Article history:
Received 13 May 2014
Received in revised form
27 July 2014
Accepted 2 August 2014
Available online 15 August 2014

Keywords:
Continuous glucose monitoring
CGM
Optical sensor
Porphyrin
Insulin infusion
Implantable glucose sensor

ABSTRACT

A new measurement system enables combination of continuous glucose monitoring (CGM) and insulin infusion. A sensor system comprising an optical glucose biosensor and an optical oxygen sensor is integrated into the insulin infusion catheter of an insulin pump. Both sensors rely on near infrared (NIR) phosphorescent porphyrin dyes, wherefore the signals can be read out transcutaneous and non-invasively with a custom-built phase fluorometer measurement module. The spectral properties of the indicator dyes and the optical setup of the measurement module were optimized to enable independent read-out in two channels. Dynamic ranges from 0 mmHg to 160 mmHg oxygen and 0 mg/dL to 360 mg/dL glucose (LOD 2 mg/dL) are covered by the oxygen and the glucose sensor, respectively. *In-vivo* measurements in pigs demonstrate good correlation of reference blood glucose levels and glucose values obtained with the presented sensor system. The evaluation of the clinical accuracy of the system with Clarke Error Grid Analysis showed similar results to CGM-devices currently on the market.

1. Introduction

Diabetes mellitus is a group of complex metabolic diseases resulting from a total or partial lack of insulin. According to the World Health Organization (WHO) approximately 347 million people worldwide suffer from diabetes (WHO, 2013). Continuous glucose measurement and adapted insulin delivery are necessary to achieve good glycemic control, normalize the diabetic's glucose metabolism and decrease the danger of acute and long-term complications of type 1 diabetes (T1D). Currently diabetics self-monitor their blood glucose level by obtaining a finger-prick sample of capillary blood, which they apply to a test strip and portable meter for analysis. This painful procedure is carried out several times a day and may result in cornification and diminished sensibility of the fingers. Moreover, episodes of hypo- or hyperglycemia that occur at night or between sampling can be missed. It has been shown that CGM is highly beneficial for children with T1D (Lagarde et al., 2006) but also for adults with T1D and nocturnal hypoglycemic events (DeVries et al., 2004; Weinzimer et al., 2008; Wentholt et al., 2007). CGM is not achievable with the currently popular therapy, as diabetic patients do not tolerate a more frequent measurement. The research of last decades was aimed at the development of a closed loop system and an artificial pancreas with automated continuous glucose measurement and adjusted insulin delivery. The MiniMed Paradigm® REAL-Time Revel™ System (Medtronic, 2014a) or the MiniMed® 530G with Enlite® (Medtronic, 2014b) are examples for commercially available insulin pumps with integrated CGM-system. Other CGM-systems on the market are the Seven®Plus (Dexcom, 2012), the FreeStyleNavigator II (Abbott Diabetes Care, 2013) or the GlucoDay®S (A. Menarini Diagnostics, 2014).

Compared to conventional (*e.g.* amperometric) glucose sensors, optical sensors benefit from the absence of electromagnetic interferences, simple design and handling as well as low cost. Miniaturization of optical sensors is easily achievable without compromising performance and dramatically reduces repulsion reactions. Evidently, optical sensing technology can provide an interesting alternative to more established electrochemical sensors and will contribute to better flexibility concerning the design of CGM-systems, their cost, materials used, *etc.*

Several schemes for optical glucose monitoring have been reported (Pickup et al., 2005; Borisov and Wolfbeis, 2008; Steiner et al., 2011). Examples are affinity sensors based on natural receptors like concanavalin A (Ballerstadt and Schultz, 2000;

* Corresponding author. Tel.: +43 316 873 32500; fax: +43 316 873 32502.
E-mail address: klimant@tugraz.at (I. Klimant).

http://dx.doi.org/10.1016/j.bios.2014.08.012
0956-5663/

Cummins et al., 2013) or synthetic receptors like boronic acids (Mader and Wolfbeis, 2008), as well as fluorescent hydrogels (Heo et al., 2011) or enzymatic biosensors which rely on glucose oxidase (GOx). In contrast to affinity sensors, enzymatic glucose sensors are distinguished by a very high selectivity (Pasic et al., 2007) and are virtually "blind" to other saccharides. Oxygen sensors which act as transducer in enzymatic glucose sensors are quite established (Amao, 2003; Quaranta et al., 2012) and can be read out with phase fluorometry using compact and potentially low cost devices. Adversely, tissue oxygenation affects the response of this type of sensor, making additional measurement of oxygen partial pressure (pO_2) essential (Li and Walt, 1995). This results in higher complexity of the composite glucose sensor. In order to ensure accurate compensation for oxygen fluctuations, both sensor elements (glucose and reference oxygen sensor) should be located in close proximity. Although the proof-of-concept was previously demonstrated for the combination of two fiber-optic sensors (Pasic et al., 2007), the array was rather bulky and did not include an insulin catheter. Evidently, integration of the insulin catheter and the sensor into one element allows for a significantly patient-friendlier and more compact setup. This is a challenging task since the optical glucose and oxygen sensor should be read out through the skin. The state of the art UV–vis probes are poorly suitable for subcutaneous measurements and can be applied only for proof-of-concept studies of such "Smart Tattoos" (Ballerstadt and Schultz, 2000; McShane et al., 2000). Recently much progress was achieved in the area of phosphorescent oxygen probes which absorb and emit in the so-called NIR optical window (Weissleder, 2001). This spectral region is distinguished by lower light absorption by the skin pigments, hemoglobin and water and by weaker auto-fluorescence from the tissue (Thompson, 1994).

The long-term performance of implantable sensors is usually compromised by accumulation of metabolically active cells. They accumulate on the surface of the sensor and consume glucose and oxygen at accelerated rate (Frost and Meyerhoff, 2006). Additionally, the formation of a fibrous capsule around the sensor alters glucose mass transfer. This can be solved by taking a blood sample and recalibrating the sensor after local environment has stabilized. Furthermore, the use of inexpensive optical sensors combined with insulin catheters makes it possible to overcome the complications mentioned above by replacing the sensor every 2–3 days.

In this contribution we present a system, which allows for continuous glucose measurement and simultaneous insulin infusion. An optical sensor system is integrated into the insulin infusion catheter connected to the insulin pump and requires only one injection site. Like most CGM-systems, the sensor measures glucose in the interstitial fluid (ISF), which is at equilibrium with blood glucose levels (Simonsen et al., 1994). Frequent measurements deliver more information and help to identify hypo- or hyperglycemic events, which might stay undetected with the finger-prick method. In future work the system will be expanded to an artificial pancreas with help of an algorithm controlling the insulin pump in dependence of the measured glucose levels. The almost pain-free solution is expected to greatly simplify glucose measurement for the patients and to decrease the risk of acute and long-term complications conditional on diabetes.

2. Material and methods

2.1. Materials

Glucose oxidase (EC 1.1.3.2 from *Aspergillus niger*, 200 U/mg), 4-tert-butylstyrene, aluminum oxide type CG-20, sodium dodecyl sulfate and 2,2′-azobis(2-methylpropionitrile), divinyl-benzene, glutaraldehyde (25% aqueous solution), poly(styrene) (average Mw 250,000) and ethylcelullose (48.0–49.5% ethoxyl basis) were purchased from Sigma-Aldrich (www.sigmaaldrich.com). Albumin fraction V from bovine serum, D-(+)-glucose and all solvents were obtained from Roth (www.carlroth.at), nitrogen and synthetic air (all of 99.999% purity) from Air Liquide (www.airliquide.at) and hydrogel HydroMed D4 (AdvanSource Biomaterials, 2010) from AdvanSource (www.advbiomaterials.com). Deionized water was used for the preparation of all aqueous solutions.

The luminescent dye platinum(II)-*meso*-tetra(4-fluorophenyl) tetrabenzoporphyrin was synthesized according to Borisov et al. (2009). The synthesis of platinum(II)-6-aza-13,20,27-triphenyltetra(tert-butylbenzo)-porphyrin is described in Supporting information. The 20% glucose solution Glucosteril® and a 0.9% physiological NaCl-solution for *in-vivo* tests were purchased from Fresenius Kabi (www.fresenius-kabi.de) and the insulin Novorapid 100 U/mL from Novo Nordisk (www.novonordisk.com).

Polytetrafluoroethylene-tubes were purchased from Bola (www.bola.de) and poly(ethylene glycol terephthalate)-foil (Mylar®) from Goodfellow (www.goodfellow.com). Intravenous catheters Tro-Venocath 3+ were obtained from Troge Medical (www.trogemedical.de).

2.2. Preparation of poly-tert-butylstyrene-particles (ptBS)

Prior to the polymerization, 4-tert-butylstyrene (tBS) and divinylbenzene (DVB) were cleaned on an aluminum oxide column to remove the inhibitor. 10.9 mL of tBS and 2.8 mL of DVB were mixed and added to 400 mL of a 0.25% (w/v) aqueous solution of sodium dodecyl sulfate (SDS). The mixture was homogenized for 2 min with a homogenizer (Miccra D1, Gerber Instruments, Switzerland) and for 5 min in an ultrasonic bath (Transsonic Digital S, Elma, Germany). The resulting emulsion was transferred into a 1 L-two-necked round-bottom flask and stirred under strong nitrogen flow for 40 min. 200 mg of 2,2′-azobis(2-methylpropionitrile) were added and the emulsion was warmed to 95 °C. After approximately 7 h, the reaction mixture was cooled to room temperature and transferred into a beaker. 600 mL of acetone were added under stirring to precipitate the resulted cross-linked polymer particles. The dispersion was centrifuged at 4000 rpm for 5 min (Rotofix 32, Hettich, Germany). For cleaning, the precipitate was suspended in approximately 60 mL of a solvent, ultrasonicated for 10 min and centrifuged again. This cleaning procedure was carried out three times with acetone, twice with a mixture of acetone, ethanol and water (2:1:1 v/v) and twice with ethanol. The particles were dried overnight in a drying oven (ED115, Binder, Germany) at 60 °C and the product (ptBS) was then homogenized in a mortar.

2.3. Staining of ptBS-particles

A solution of 5 mg platinum(II)-*meso*-tetra(4-fluorophenyl)tetrabenzoporphyrin (PtTPTBPF) in 6 mL chloroform was slowly added to a 10% (w/v) dispersion of ptBS in $CHCl_3$. The mixture was stirred for 15 min and ultrasonicated for another 15 min. The solvent was removed by evaporation under nitrogen flow. The stained PtTPTBPF–ptBS-particles were dried overnight at 60 °C and then homogenized in a mortar.

2.4. Preparation of the glucose biosensor

The surface of the polytetrafluoroethylene (PTFE)-tube simulating the insulin infusion catheter was activated shortly before the coating procedure by oxygen plasma etching (FEMTO UHP, Diener Electronic, Germany). The process was carried out at a basic pressure of 0.3 mbar and a plasma power of 100 W and 40 kHz for 60 s.

A 1.25% aqueous glutaraldehyde solution was added to a 10% (w/v) aqueous solution of GOx and bovine serum albumin (BSA) (ratio 1:2 v/v). This enzyme solution was spray-coated onto the plasma-etched catheter tube with an ultrasonic frequency of 25 kHz, a vaporizer power of 2.2 W and a focusing air flow of 20 mbar. The coating procedure was carried out with a flow of 0.1 mL/min at a distance of 33 mm for 6 s. The cross-linking took place spontaneously at room temperature during drying for 30 min.

5 g of ethylcelullose (EC) and 2.5 g of hydrogel HydroMed D4 were dissolved in 100 g of a mixture of ethanol and water (ratio 9:1 v/v). 20 mg of PtTPTBPF–ptBS dye-particles were dispersed in 100 μL of the opaque EC-D4-solution. This solution was further diluted 1:2 with a mixture of ethanol and water (ratio 9:1) for spray-coating on top of the dried enzyme-layer with a vaporizer power of 4 W. The distance between nozzle and catheter was 50 mm and the coating time was 10 min at a flow of 0.05 mL/min.

The thickness of the sensing layer was determined on a bright field and a fluorescence microscope. Therefore, the catheters were mounted in a cold-setting two-component epoxy resin (Epofix™, *www.struers.de*). After curing at 24 °C, the samples were ground (up to 4000 grit), polished with a diamond suspension (up to 0.25 μm) and sliced.

2.5. Preparation of the reference oxygen sensor

5 mg of platinum(II)-6-aza-13,20,27-triphenyltetra(tert-butyl-benzo)-porphyrin (tbutPtNTBP) and 50 mg of polystyrene (PS) were dissolved in 450 mg of toluene. This solution was spray-coated onto the catheter, which already carried the glucose sensor. To prevent contamination of the glucose sensor, it was covered with a piece of plastic foil during spray-coating of the reference oxygen sensor.

2.6. In-vitro characterization

A customized flow-through cell for five sensors was used for continuous flow-analysis of the sensor response to different glucose concentrations in a physiological relevant range. A glucose concentration profile was carried out in step gradients from 0 mg/dL to 360 mg/dL and back down to 0 mg/dL. The aqueous glucose solutions were kept at constant temperature in a cryostat (DC50, Thermo Haake, Germany). The oxygen content of the solutions was adjusted by purging defined mixtures of nitrogen and synthetic air through the solutions using a gas-mixing device (MFC, MKS instruments, Germany).

After completion of the step gradient, the glucose concentration was alternated between 45 md/dL and 360 mg/dL over a period of 50 h for identification of a sensor drift at low and high glucose concentrations.

2.7. In-vivo experiments

All *in-vivo* experiments were carried out in pigs in consent with Directive 2010/63/EU on the protection of animals used for scientific purposes and were approved by the ethics commission of the Austrian Federal Ministry for Science and Research (BMWF-66.010/0117-II/3b/2011). Test objects were healthy house pigs (25–30 kg) which were under general anesthetics, monitored and provided artificial respiration during the experiments.

In order to achieve glucose concentrations in a physiologically relevant range, a glucose-clamp experiment was conducted under hyperinsulinemic conditions. For this purpose, a medical glucose solution was infused intravenously to achieve different blood glucose concentrations (hypo-, normo- and hyperglycemia) in a range from 35 mg/dL to 300 mg/dL glucose. Arterial blood samples were taken every 5 min to obtain reference values for blood glucose concentration and oxygen partial pressure (Skjaervold and Aadahl, 2012). Reference measurements were carried out with a Super GL2 (HITADO GmbH, Germany) and a GEM premier 3000 (Instrumentation Laboratory, Belgium).

The steel cannula of a commonly used intravenous catheter was placed subcutaneously into the pig's sides. When the cannula was removed, the coated catheter remained in the tissue and was fixed with medical tape to avoid accidental removal. The measurement module was positioned on the pig's skin above the sensor. Basal (2.4 U/h) and bolus insulin (25 μL/2.5 min) as well as equivalent amounts of physiological NaCl-solution were infused through the catheter in order to investigate the effects of insulin and NaCl-solution on the sensor signal. Catheters without infusion served as reference.

2.8. Sterilization

10 glucose sensor elements were sterilized with electron-beam sterilization (25 kGry), 10 were γ-sterilized (25 kGry) and another 10 served as reference without sterilization. All 30 sensors were tested *in-vitro* in a continuous-flow-setup regarding to their response to glucose in a range from 0 mg/dL to 360 mg/dL glucose.

2.9. Cytotoxicity studies

The glucose and oxygen sensor solutions were knife-coated onto Mylar®-foil to obtain an approximately 2.5 μm-thick layer after evaporation of the solvents. According to ISO-guidance (ISO1993-5, 2009; ISO10993-12, 2009) for indirect cytotoxicity tests, 3 cm^2 of the knife-coated sensors were extracted with 1 mL

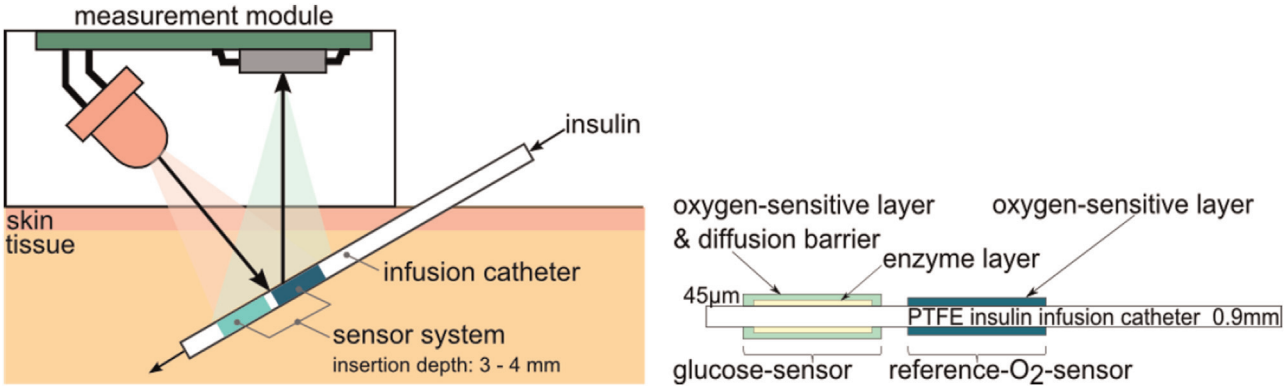

Scheme 1. Cross-sections of the sensor system (left) and of the catheter with integrated optical sensor system (right).

medium at 37 °C. The human fibroblast cell line MRC-5 was exposed to the diluted and undiluted extracts for 24 h, 48 h and 72 h before cell vitality was tested with formazan bioreduction.

3. Results and discussion

3.1. Sensor system

The sensor system consists of two sensor elements-an optical glucose biosensor and an optical reference oxygen sensor, which are located on adjacent sections of an insulin infusion catheter (Scheme 1).

The glucose sensor consists of an enzyme layer and an oxygen-sensitive layer. The bottom layer is prepared by cross-linking GOx with BSA using the bifunctional reagent glutaraldehyde. The stability of the enzyme is maintained when immobilized by crosslinking with BSA (Chuanxin et al., 2009). An excess of the enzyme GOx is immobilized, compensating for a possible loss of activity.

Oxidation of glucose catalyzed by GOx occurs according to the following equation: β-D-Glucose + O_2 + H_2O $\xrightarrow{GOx}$ D-Glucono-β-lactone + H_2O_2. The oxygen-sensitive phosphorescent dye-particles in the upper layer act as a transducer for the rate of oxygen consumption. A mixture of polyurethane hydrogel D4 and ethyl cellulose acts as support and matrix for the oxygen-sensitive particles. It acts as diffusion barrier for glucose but not for oxygen, which is favorable due to the low ratio of glucose to oxygen in tissue. The biocompatible hydrogel contains about 50% of water and is highly permeable to glucose. On the contrary, the significantly more hydrophobic ethyl cellulose slows the diffusion of glucose, hence reducing the enzymatic conversion and shifting the dynamic range of the glucose sensor. It ensures, that the sensor response is limited by mass transfer rather than by the enzymatic reaction and prevents additional local oxygen depletion by oxygen consumption of the sensor.

The reference oxygen sensor consists of a second phosphorescent dye in polystyrene coated directly onto the catheter and is used for compensation of the oxygen cross-talk of the glucose biosensor. The obtained signal is the difference between the oxygen levels (ΔpO_2) measured by the two sensor elements. The oxygen level resulting from oxygen consumption by the enzymatic reaction (glucose sensor) is subtracted from the local oxygen partial pressure (reference oxygen sensor).

The catheter used in the presented system is made from polytetrafluoroethylene. This polymer is commonly applied in commercial insulin infusion catheters and other medical products due to its high chemical inertness and a very low friction coefficient, preventing the adhesion of biological components.

3.2. Oxygen indicators

The indicators used in the sensor system should fulfill the following requirements: (i) absorb and emit in the "NIR optical window" to be suitable for subcutaneous read-out; (ii) possess significantly different spectral properties or luminescence decay times to provide unbiased information from the two sensor elements; (iii) have good phosphorescence brightness to ensure sufficient signal to noise ratio; (iv) be covalently grafted into the polymers or be highly lipophilic to avoid leaching from the sensing material. Unfortunately, dyes that can fulfill these requirements are very rare (Xiang et al., 2013). Platinum(II) and palladium(II) complexes with tetrabenzoporphyrins (Vinogradov and Wilson, 1995; Finikova et al., 2004), tetranaphthoporphyrins (Finikova et al., 2003; Sommer et al., 2009) and aza-tetrabenzoporphyrins (Borisov et al., 2010) show sufficiently bright NIR-phosphorescence, whereas numerous highly

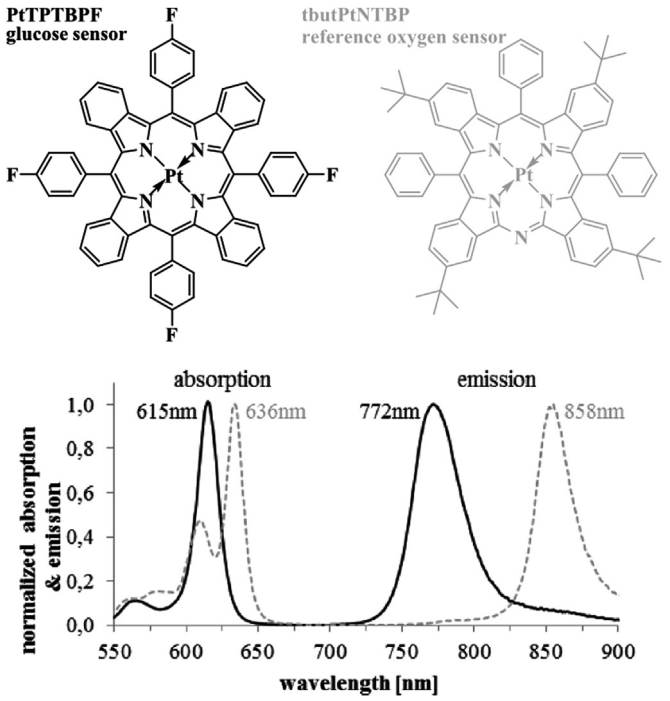

Fig. 1. Chemical structures of the indicators and their spectral properties in toluene.

fused porphyrinoids absorb too far in the NIR and are not emitting (Mori et al., 2013). Naphthoporphyrins and their molecular hybrids with benzoporphyrins suffer from rather poor photostability (Niedermair et al., 2010). Therefore, very photostable platinum(II) complexes with tetrabenzoporphyrins (Borisov et al., 2008) and aza-tetrabenzoporphyrins (Borisov et al., 2010) were obvious candidates for application in the presented sensor system. The platinum(II) complex with *meso*-tetra(4-fluorophenyl) tetrabenzoporphyrin (PtTPTBPF) is used for the glucose biosensor. It is excitable with a 615 nm light emitting diode (LED) and emits in the NIR region (Fig. 1). The luminescence brightness (defined as the product of the molar absorption coefficient ε and the luminescence quantum yield Φ) of the platinum(II) complexes with aza-tetrabenzoporphyrins are significantly lower than that of PtTPTBPF. Therefore, a higher concentration of the aza-benzoporphyrin is necessary to achieve comparable signals. Since the reported dyes possess limited solubility, we prepared a new highly soluble platinum(II)-6-aza-13,20,27-triphenyltetra(*tert*-butylbenzo)-porphyrin (tbutPtNTBP, Fig. 1). Four *tert*-butyl groups render the dye excellently soluble in common organic solvents and in polymers such as polystyrene. The photophysical properties of the dye are preserved even at very high concentrations (10% w/w of the dye in polystyrene), indicating that the dye does not aggregate under these conditions. Both absorption and emission of tbutPtNTBP are significantly different from those of PtTPTBPF (Fig. 1), ensuring good separation of the sensor signals upon dual excitation and detection in two emission channels. Although excitation of both dyes with a single light source is theoretically possible, it would result in noticeable interference of PtTPTBPF-emission in the tbutPtNTBP-window. The molar absorption coefficients of tbutPtNTBP are very high: 159,000 $M^{-1}\,cm^{-1}$ (Q-band, 636 nm) and 128,000 $M^{-1}\,cm^{-1}$ (Soret-band, 408 nm). The quantum yield of NIR phosphorescence (λ_{max} = 858 nm) is moderate (12%). Importantly, the photostability of the new complex is sufficiently high (Figs. S7 and S8) despite the presence of electron-donating tertiary butyl groups. In fact, even at high dye concentrations thousands of measurement points can be acquired, resulting in only a small drift of the luminescence decay time. Moreover, the intensity of excitation

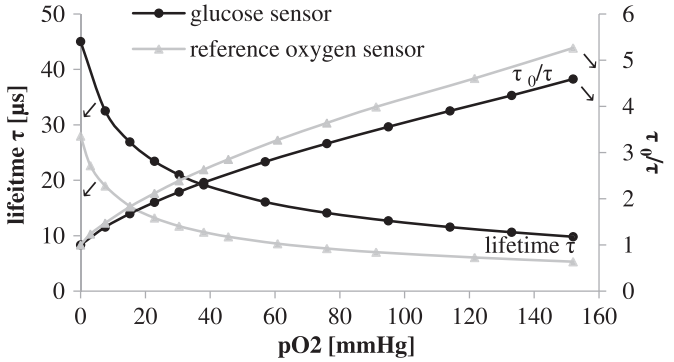

Fig. 2. Lifetime and Stern–Volmer plot for the glucose and the reference oxygen sensor at 25 °C.

light reaching the sensor is about 100 times lower in *in-vivo* measurements, making potential photobleaching effects negligible during the whole operation time of the sensor.

The long-lived phosphorescence of the platinum(II) complexes is effectively quenched by molecular oxygen (Fig. 2) in solutions and in polymers. The sensor elements show optimal response in the dynamic range from 0 mmHg to 160 mmHg. Quantification at higher pO_2 is also possible albeit with lower resolution. A modified Stern–Volmer equation adapted from the so-called two site model (Carraway et al., 1991) can be used to adequately fit the non-linear Stern–Volmer plots (τ_0/τ vs. pO_2):

$$\frac{\tau}{\tau_0} = \frac{f_1}{1 + K_{SV1} \cdot pO_2} + \frac{f_2}{1 + K_{SV2} \cdot pO_2} \quad (1)$$

where τ is the lifetime at a given oxygen concentration (pO_2), τ_0 is the lifetime under anaerobic conditions, f_1 and f_2 are the fractions of the total emission for each of the two environments (with $f_1+f_2=1$), and K_{SV1} and K_{SV2} are the Stern–Volmer constants for each component.

3.3. Coating of the sensor elements

The coating of the sensor elements onto the catheter is a crucial step. In order to achieve a satisfactory adhesion of the sensor materials to the PTFE–catheter, the catheter surface was activated by oxygen plasma etching shortly before the coating procedure. Different coating methods for deposition of the sensor materials onto the PTFE catheter were examined. Spray-coating was favored to other methods (*e.g.* dip-coating, manual deposition and inkjet printing) due to good reproducibility and better suitability for coating the two sensor elements on adjacent sections of the catheter by using a covering mask. Other selection criteria were simplicity of the method and possibility for easy upscaling.

Microscopic examination of the coated sensors showed good adhesion of the sensor material on the catheter. Layer thicknesses were found to be homogeneous. The glucose sensors (45 ± 7 µm), for example, is made up of an approximately 32 µm thick oxygen-sensitive layer and an approximately 13 µm thick enzyme layer. All coated catheters survived storage in physiological NaCl-solution for 5 days, exceeding the planned period of use of 3 days. Furthermore, insertion of the catheter into subcutaneous tissue is a critical step since the sensor materials might be detached. In *in-vitro* experiments, the catheters were inserted into and removed from a piece of beef meat several times. The plasma-etched catheters showed satisfactory adhesion of the sensor materials whereas the sensors were removed rather easily when the catheter's surface was not activated. The same results were obtained in *in-vivo* experiments in pigs.

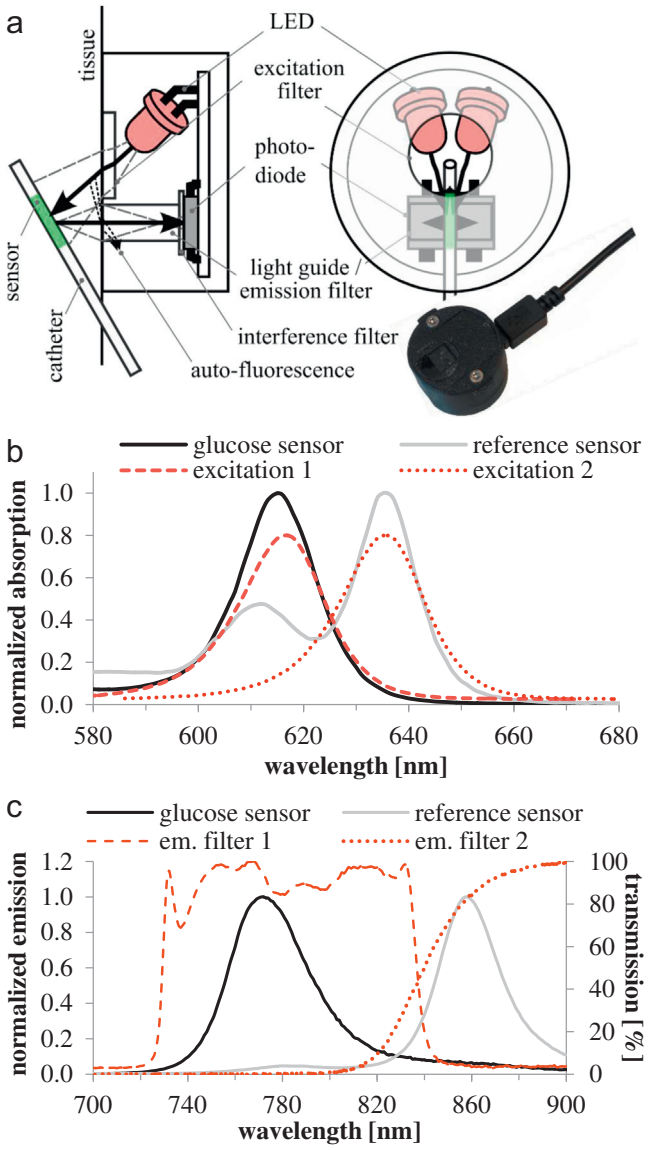

Fig. 3. (a) *BiLuMOS* read-out module and its components; (b) absorption spectra of the indicators in the two sensor elements and the emission spectra of the LEDs used for the excitation of the indicators; (c) emission spectra of the indicators and transmission spectra of the respective optical filters.

3.4. Read-out module

A module for read-out of the sensor should fulfill the following requirements: (i) be small enough for comfortable measurement directly on the patient's skin; (ii) contain two separate channels for interrogation of the glucose and the reference oxygen sensor; (iii) effectively guide the excitation light and collect the emission light and simultaneously reduce the received background light; (iv) have simple design and rely on cheap optoelectronic components. Keeping these requirements in mind, we manufactured a novel miniaturized phase fluorometer termed *BiLuMOS* (*Bi-Lu*minescence *M*easurement of *O*ptical *S*ensors), which is shown schematically in Fig. 3.

The two channels are optimized for the read-out of tbutPtNTBP and PtTPTBPF and include a pair of different LEDs, excitation and emission filters (Fig. 3b). The LEDs are tilted by 45°/15° and are offset to match exactly the sensor system on the catheter, which must be inserted 3–4 mm deep into the tissue. Both photodiodes are placed next to each other with their optical paths separated.

This position over the catheter is not optimal but is compensated by the fact that no beam splitting is required for the different emission wavelengths. This would be necessary if just one optimal aperture was used for both detectors and would result in additional transmission losses at the beam splitter. The fixed position of the sensor system with respect to the measurement module allowed for shortening the light paths from the LED *via* the sensor to the photodiode, hence increasing light collection efficiency, suppressing background light and minimizing the amount of optical components.

The emission filters on top of the photodiodes act as waveguides as they are surrounded by air. They increase the aperture for the emission light and simultaneously reduce the amount of background light (auto-fluorescence). All filters used are relatively low-cost and aim at a good signal separation. Both channels use a Calflex-filter (Schott, Austria) on the excitation side. The emission filter set 1 (glucose sensor) consists of a custom-made band-pass filter and an RG9 long-pass filter (Schott, Austria) whereas the emission filter set 2 (reference oxygen sensor) is made up of an RG830 filter (Schott, Austria) and a Special-Medium-Blue band-pass filter (Lee, USA). As can be seen in Fig. 3c, there is a crosstalk between the two channels. Narrower interference filters could further improve separation of the emissions from the two indicators.

Further information on the measurement electronics, the measurement module and the measurement principle of phase fluorometry can be found in Supplementary data.

3.5. In-vitro characterization

Fig. 4a shows the fully reversible response of the glucose sensor to different analyte concentrations with a detection limit (LOD) of 2 mg/dL. A dynamic range from 0 mg/dL to 360 mg/dL is achieved, covering the physiological relevant ranges of hypo- (<40 mg/dL), normo- and hyperglycemia (>140 mg/dL). The dynamic range of the presented sensor is currently being optimized to achieve a more linear response expanded to higher glucose concentrations since hyperglycemic excursion of diabetic patients can exceed 360 mg/dL.

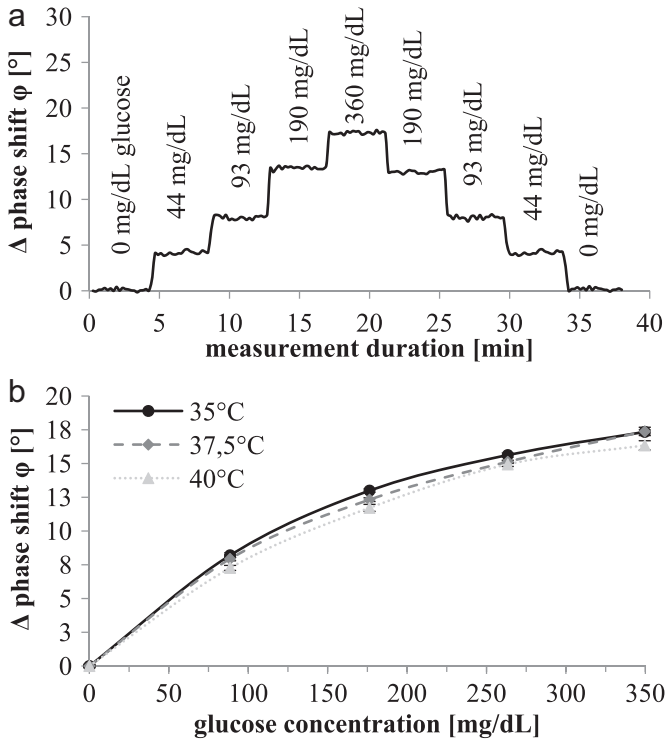

Fig. 4. Dynamic reversible response of the glucose sensor to the analyte: (a) continuous-flow measurements in air-saturated aqueous glucose solutions at 25 °C and (b) temperature dependency of the sensor's response to glucose.

The glucose sensor shows acceptable stability over a measurement period of 50 h with a sensor drift of $+0.13$%/h of the initial sensor signal at 360 mg/dL and -0.38%/h at 45 mg/dL. The sensor drift describes the analyte-independent signal change as percentage of the initial signal with time. This sensor drift could be compensated for by recalibration of the sensor after 24 h. The glucose sensor can be stored at 4 °C for several weeks without noticeable change in the sensitivity, which is due to a surplus of enzyme and high stability of the cross-linked enzyme. The response time t_{90} (defined as the time needed for a signal change from 0% to 90% of the signal maximum) is 60 ± 10 s, which is fast enough for CGM.

The glucose biosensor shows only minor response to temperature in the physiologically relevant range between 35 °C and 40 °C (Fig. 4b). The origin of the temperature crosstalk is rather complex since temperature affects the diffusion rates of glucose and oxygen, the rate of the enzymatic oxidation of glucose and the sensitivity of the oxygen transducer. Since the implanted sensor system will be shielded from changes in ambient temperature by the surrounding tissue, the skin as well as by the measurement module the temperature crosstalk is expected to be negligible.

Fig. 5 shows the response of the oxygen and the glucose sensor to the analytes oxygen and glucose. The reference sensor only responds to oxygen (Fig. 5a), which indicates that there are no optical interferences from the glucose sensor in the detection channel of the oxygen sensor. On the other hand, the response of the glucose sensor depends both on the concentration of glucose and pO_2, which can be deducted from the mechanism of the enzymatic reaction. The data confirm the necessity of a reference oxygen sensor for glucose quantification. Evidently, the sensor is suitable for glucose measurements in the investigated range from 45 mmHg to 160 mmHg. The mean concentration of intercellular oxygen is 56.3 ± 3.9 mmHg and fluctuations of up to 15.8 mmHg of the subcutaneous pO_2 are possible (Simonsen et al., 1994). The calibrations of the individual sensors can be combined (Fig. 5c) to result in the dependency of ΔpO_2 (defined as the difference of pO_2 values obtained by both sensors).

3.6. Optimization of the sensor insertion depth

In a preliminary study, an optical setup (Fig. 6) was realized to simulate *in-vivo* read-out of the glucose sensor element using a combination of beef meat and fat. Beef meat was used for simulation of tissue and skin with blood supply. The damping effect of myoglobin present in the muscle tissue is expected to be similar to that of hemoglobin during *in-vivo* measurements. Beef fat was used for imitation of fluorescence scattering. A 2 mm² planar sensor spot was positioned beneath meat layers with thicknesses between 2.5 mm and 10 mm to examine the relation between signal loss and the insertion depth.

The observed background light is composed of the auto-fluorescence of tissue components, scattered and reflected light. The influence of background light on the sensor signal (luminescence decay time) can be compensated for mathematically. Lifetime measurements with two-frequency-correction (Borisov et al., 2006) lead to confidential results for layer thicknesses up to 5 mm (Table 1). In fact, the calculated decay times (which reflect the degree of oxygenation) are identical to those for the sensor without the tissue. Similar results were obtained for *in-vivo* measurements in pigs (data not shown). As can clearly be seen in Table 1, the two-frequency correction reaches its limits when the signal to noise ratio is low. The lifetime measurement becomes

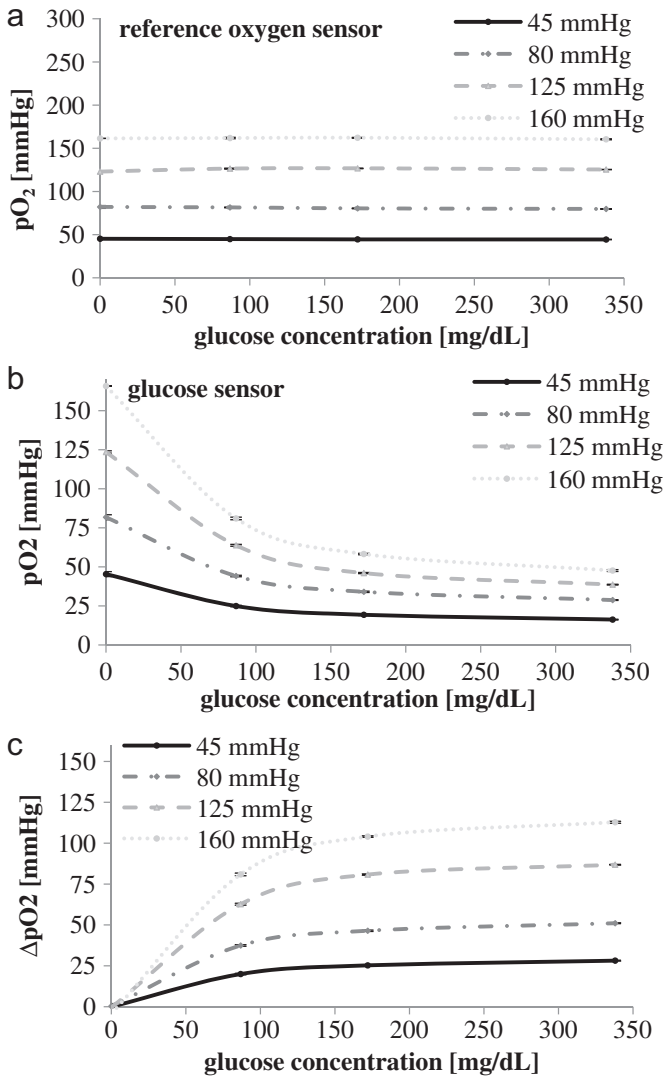

Fig. 5. Response of the reference oxygen sensor (a) and the glucose sensor (b) to both analytes. Calculated response for the difference of pO_2 values for the two sensors (c).

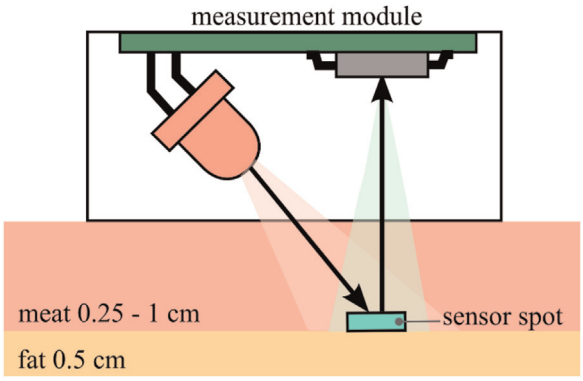

Fig. 6. Scheme of system setup simulating absorption and scattering in tissue.

unreliable at a meat layer thickness of 10 mm (~ 50% background light), which is evident from a significantly decreased value of the calculated luminescence lifetime (Table 1).

This limitation could probably be overcome with time-resolved measurements, which enable a complete elimination of the short-lived background after a short delay of several microseconds. This alternative measurement method would require alterations in the electronics of the read-out module and was therefore not performed in the current work. Nevertheless, it can be concluded, that reliable measurements of phosphorescence lifetime and hence oxygenation are possible through skin and tissue with the setup used and with the sensor system placed at moderate insertion depth.

Table 1
Dependency of the signal intensity and calculated luminescence lifetime on the insertion depth of the sensor.

Meat layer thickness [mm]	Background signal [%]	Relative signal intensity [%]	Lifetime τ [μs][a]
0	< 0.01	100.0 ± 8.8	22
2.5	3.5 ± 0.1	40.6 ± 0.2	22
5	2.6 ± 0.1	19.5 ± 0.1	22
10	2.8 ± 0.1	5.9 ± 0.1	10

[a] Calculated with two-frequency-correction algorithm.

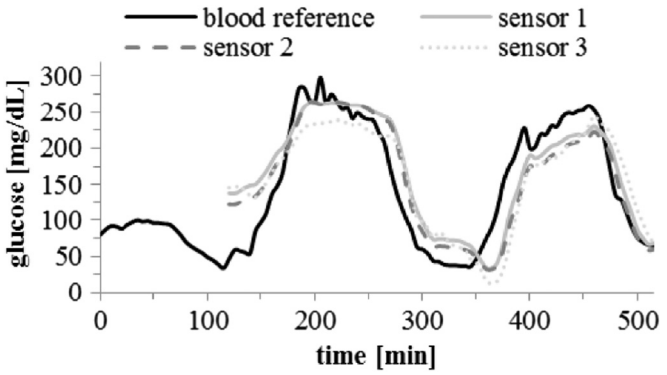

Fig. 7. Results of *in-vivo* experiment: comparison of reference blood glucose levels with system-generated data (120 min run-in time).

3.7. In-vivo experiments

The aspired experimental goal was to show the stability and accuracy of the new setup comparing it to reference measurements in whole blood. The clinical accuracy of the presented system was evaluated with the Clarke Error Grid Analysis (EGA) (Clarke et al., 1987; Clarke, 2005). A two-point calibration (aerobic: 21% oxygen and anaerobic: 0% oxygen) was made for each sensor element before implantation. The oxygen-compensated data (ΔpO_2) was evaluated retrospectively (not online) by comparing it to the concentration of analyte measured in blood. Fig. 7 compares interstitial fluid glucose levels obtained with three optical glucose sensors with the reference blood glucose values. A warm-up time of 120 min is required as implantation of the catheter can cause tissue trauma or hemorrhage, changing the tissue's physiology around the sensor (Klueh et al., 2011). During this time reliable measurements for glucose monitoring are not possible and are therefore not shown in Fig. 7.

Obviously, the new optical system is suitable for continuous glucose monitoring. The system-generated data follows the blood glucose levels with a time-delay, comparable to time lags between 2 min and 22 min, which have been reported for different commercial CGM-systems (Davey et al., 2010; Garg et al., 2010; Joubert and Reznik, 2012). Physiological and system-conditional lag times between the blood glucose level and the glucose level in interstitial fluid were not taken into consideration when carrying out

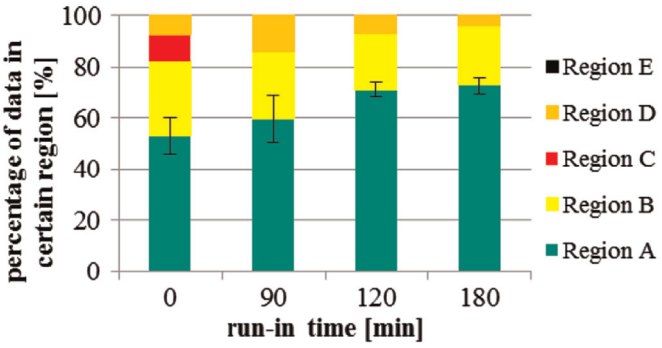

Fig. 8. Results of Clarke Error Grid Analysis depending on run-in time.

the EGA (Fig. 8). Such correction would further improve the results.

Different run-in times were taken into consideration when carrying out the EGA. Data presented in Fig. 8 origins from a set of three sensors measured *in-vivo*. Error bars are only shown for data in region A of the error grid to keep the diagram simple but are in a similar range for all regions. With no run-in time, 80% of all data lie in regions A and B and 0% in region E. An elongation of the run-in time improves these results. After a warm-up time of 120 min 95% of all data lie in regions A and B, undermatching the mean warm-up time of commercial CGM-systems with 175 min (Klueh et al., 2011).

Simultaneous infusion of insulin and physiological NaCl-solution showed no significant effect on the sensor′s behavior. Results are published elsewhere (Hajnsek et al., 2014). Lindpointner et al. (2010a, 2010b) and Hermanides et al. (2008) have suggested similar. It can therefore be concluded that insulin infusion and glucose measurement can be combined in one catheter, which is an essential improvement of actual possible therapy options for type I diabetes and would be broadly accepted.

3.8. *Biocompatibility and sterilization of the sensors*

Biocompatibility of the sensors is mandatory for their medical applications. It was assessed with the recommended ISO tests. The cell vitality (dehydrogenase activity) of the diluted and undiluted extracts was compared to the cell vitality of the control (Fig. S10). Since the eluates from the sensor material showed no significant decrease of dehydrogenase activity at any tested point of time, the oxygen-sensitive layers of both sensor elements can be classified as non-cytotoxic according to the ISO-guidelines for medical products.

Metal-free porphyrins and their complexes belong to efficient photosensitizers of singlet oxygen and therefore may be phototoxic (Bonnett, 1995; Sternberg et al., 1998). Due to the short decay time of singlet oxygen in water (~3 μs, Schiller and Müller, 1991) phototoxic effects are significant only for very small objects such as porphyrin conjugates (Chen et al., 2004; Hirohara et al., 2009) or dye-doped nanoparticles (Choi et al., 2011; Shi et al., 2014). In our work the porphyrin indicators are embedded into hydrophobic polystyrene-based polymers, ensuring efficient deactivation of singlet oxygen due to a long diffusion pathway and a short singlet oxygen lifetime (Schiller and Müller, 1991). Notably, the highly lipophilic dyes are excellently compatible with the hydrophobic polystyrenes and do not show any leaching in aqueous media.

Considering the glucose biosensor, a potential negative effect may be caused by hydrogen peroxide (H_2O_2) produced during enzymatic oxidation of glucose. H_2O_2 can cause local irritation of the tissue located in proximity of the sensor and may lead to inflammation (Schalkwijk et al., 1986; Halliwell et al., 2000). Addition of the enzyme catalase, which promotes decomposition of hydrogen peroxide to oxygen and water, may minimize this effect and is currently being investigated.

Sterilization of the sensors before applications in humans is another critical issue. In medical technology, four different sterilization techniques are commonly used: chemical sterilization with ethylene oxide, sterilization by irradiation (γ- and electron-beam-sterilization) and steam-pressure sterilization. Both chemical and steam-pressure sterilization are performed under harsh conditions and are expected to reduce the activity of GOx dramatically. Sterilization by irradiation is more promising and can be performed for the product in its final outer package without the need for additional process steps. As was previously demonstrated (Zajko and Klimant, 2013) different doses of radiation of γ- and β-beams (15, 25, 50 kGry) do not affect the absorption and emission properties of the oxygen indicator. A radiation dose of 25 kGry was chosen for sterilization of the glucose sensor since this dose is commonly used for sterilization of medical devices. These experiments revealed that GOx is still active after both β- and γ-sterilization with 25 kGry. The radiation exposure during γ-sterilization caused changes in the sensors′ response, while effects were negligible when using β-sterilization. It can be concluded that sterilization by β-radiation is the preferable method for the enzymatic glucose biosensors.

4. Conclusions

We presented a new sensor system for continuous glucose monitoring in interstitial fluid. The system relies on the combination of two optical sensors (a glucose biosensor and a reference oxygen sensor) based on two near-infrared phosphorescent indicators. It was shown that the sensors coated onto the surface of the insulin catheter can be read out through the skin using a new compact and low-cost 2-channel phase fluorometer. The glucose levels obtained with the sensor-sytem show good correlation with reference blood glucose values. The sensors can be sterilized by β-radiation without significant effect on the response. Linearization of the response to glucose *via* optimization of the thickness and composition of the diffusion layer is expected to simplify the calibration procedure and is currently being investigated. Further improvements include optimization of the optical setup and the indicator chemistry to achieve even better separation of the luminescent signals from both sensors. It can be concluded that this work paves the way to development of an artificial pancreas with automated continuous blood glucose measurement and adjusted insulin delivery.

Acknowledgments

We gratefully acknowledge the funding by the Austrian Federal Ministry for Transport, Innovation and Technology (project iKath) and the support of the Institute of Biomedical Research at Medical University of Graz during the animal experiments.

Appendix A. Suppementary information

Supplementary data associated with this article can be found in the online version at http://dx.doi.org/10.1016/j.bios.2014.08.012.

References

Abbott Diabetes Care, 2013. ⟨http://www.abbottdiabetescare.co.uk/your-products/freestyle-navigator/continuous-glucose-monitoring⟩ (24.07.2014).

AdvanSource Biomaterials, 2010. HydroMed TM. (24.07.2014).
A. Menarini Diagnostics, 2014. ⟨http://www.diabetesnet.com/diabetes-technology/meters-monitors/future-meters-monitors/amenarini-diagnostics⟩ (24.07.2014).
Amao, Y., 2003. Microchim. Acta 143, 1–12.
Ballerstadt, R., Schultz, J.S., 2000. Anal. Chem. 72, 4185–4192.
Bonnett, R., 1995. Chem. Soc. Rev. 24, 19–33.
Borisov, S.M., Neurauter, G., Schroeder, C., Klimant, I., Wolfbeis, O.S., 2006. Appl. Spectrosc. 60, 1167–1173.
Borisov, S.M., Wolfbeis, O.S., 2008. Chem. Rev. 108, 423–461.
Borisov, S.M., Nuss, G., Klimant, I., 2008. Anal. Chem. 80, 9435–9442.
Borisov, S.M., Nuss, G., Haas, W., Saf, R., Schmuck, M., Klimant, I., 2009. J. Photochem. Photobiol. A: Chem. 201, 128–135.
Borisov, S.M., Zenkl, G., Klimant, I., 2010. ACS Appl. Mater. Interfaces 2, 366–374.
Carraway, E.R., Demas, J.N., DeGraff, B.A., Bacon, J.R., 1991. Anal. Chem. 63, 337–342.
Chen, X., Hui, L., Foster, D.A., Drain, C.M., 2004. Biochemistry 43, 10918–10929.
Choi, K.H., Wang, K.K., Shin, E.P., Oh, S.L., Jung, J.S., Kim, H.K., Kim, Y.R., 2011. J. Phys. Chem. C 115, 3212–3219.
Chuanxin, H., Jianhong, L., Laiyong, X., Qianling, Z., Cuihua, L., Dayong, G., Guangzhao, Z., Chi, W., 2009. Langmuir 25, 13456–13460.
Clarke, W.L., 2005. Diabetes Technol. Ther. 7, 776–779.
Clarke, W.L., Cox, D., Gonderfrederick, L.A., Carter, W., Pohl, S.L., 1987. Diabetes Care 10, 622–628.
Cummins, B.M., Garza, J.T., Cote, G.L., 2013. Anal. Chem. 85, 5397–5404.
Davey, R.J., Low, C., Jones, T.W., Fournier, P.A., 2010. J. Diabetes Sci. Technol. 4, 1393–1399.
DeVries, J.H., Wentholt, I.M.E., Masurel, N., Mantel, I., Poscia, A., Maran, A., Heine, R. J., 2004. Diabetes/Metab. Res. Rev. 20, S43–S46.
Dexcom, 2012. ⟨http://www.dexcom.com/media/dexcom-seven-plus⟩ (24.07.2014).
Finikova, O.S., Cheprakov, A.V., Beletskaya, I.P., Carroll, P.J., Vinogradov, S.A., 2004. J. Org. Chem. 69, 522–535.
Finikova, O.S., Cheprakov, A.V., Carroll, P.J., Vinogradov, S.A., 2003. J. Org. Chem. 68, 7517–7520.
Frost, M., Meyerhoff, M.E., 2006. Anal. Chem. 78, 7370–7377.
Garg, S.K., Voelmle, M., Gottlieb, P.A., 2010. Diabetes Res. Clin. Pract. 87, 348–353.
Hajnsek, M., Nacht, B., Sax, S., Klimant, I., 2014. Acta Diabetol. (In press), 10.1007/s00592-014-0578-y.
Halliwell, B., Clement, M.V., Long, L.H., 2000. FEBS Lett. 486, 10–13.
Heo, Y.J., Shibata, H., Okitsu, T., Kawanishi, T., Takeuchi, S., 2011. Proc. Natl. Acad. Sci. USA 108, 13399–13403.
Hermanides, J., Wentholt, I.M., Hart, A.A., Hoekstra, J.B., De Vvries, J.H., 2008. Diabetes Care 31, 1120–1122.
Hirohara, S., Obata, M., Alitomo, H., Sharyo, K., Ando, T., Yano, S., Tanihara, M., 2009. Bioconjug. Chem. 20, 944–952.
ISO1993-5, 2009. Biological evalua tion of medical devices part 5: Test for in vitro cytotoxicity.
ISO10993-12 , 2009. Biological evaluation of medical devices. part 12: Sample preparation and reference materials.
Joubert, M., Reznik, Y., 2012. Diabetes Res. Clin. Pract. 96, 294–305.
Klueh, U., Liu, Z., Feldman, B., Henning, T.P., Cho, B., Ouyang, T., Kreutzer, D., 2011. J. Diabetes Sci. Technol. 5, 583–595.
Lagarde, W.H., Barrows, F.P., Davenport, M.L., Kang, M., Guess, H.A., Calikoglu, A.S., 2006. Pediatr. Diabetes 7, 159–164.
Li, L., Walt, D.R., 1995. Anal. Chem. 67, 3746–3752.
Lindpointner, S., Korsatko, S., Koehler, G., Koehler, H., Schaller, R., Kaidar, R., Yodfat, O., Schaupp, L., Ellmerer, M., Pieber, T.R., Regittnig, W., 2010a. Diabetes Care 33, 595–601.
Lindpointner, S., Korsatko, S., Koehler, G., Koehler, H., Schaller, R., Schaupp, L., Ellmerer, M., Pieber, T.R., Regittnig, W., 2010b. Diabetes Care 33, 833–838.
Mader, H.S., Wolfbeis, O.S., 2008. Microchim. Acta 162, 1–34.
McShane, M.J., Russell, R.J., Pishko, M.V., Cote, L.G., 2000. IEEE Eng. Med. Biol. Mag. 19, 36–45.
Medtronic, 2014a. ⟨http://www.professional.medtronicdiabetes.com/paradigm-revel-real-time⟩ (24.07.2014).
Medtronic, 2014b. ⟨http://www.professional.medtronicdiabetes.com/minimed-530-g⟩. (24.07.2014).
Mori, H., Tanaka, T., Osuka, A., 2013. J. Mater. Chem. C 1, 2500–2519.
Niedermair, F., Borisov, S.M., Zenkl, G., Hofmann, O.T., Weber, H., Saf, R., Klimant, I., 2010. Inorg. Chem. 49, 9333–9342.
Pasic, A., Koehler, H., Klimant, I., Schaupp, L., 2007. Sens. Actuators B: Chem. 122, 60–68.
Pickup, J.C., Hussain, F., Evans, N.D., Rolinski, O.J., Birch, D.J.S., 2005. Biosens. Bioelectron. 20, 2555–2565.
Quaranta, M., Borisov, S., Klimant, I., 2012. Bioanal. Rev. 4, 115–157.
Schalkwijk, J., Van den Berg, W.B., Van de Putte, L.B.A., Joosten, L.A.B., 1986. Arthritis Rheum. 29, 532–538.
Schiller, K., Müller, F.W., 1991. Polym. Int. 25, 19–22.
Shi, H., Ma, X., Zhao, Q., Liu, B., Qu, Q., An, Z., Zhao, Y., Huang, W., 2014. Adv. Funct. Mater. 24, 4823–4830.
Simonsen, L., Bulow, J., Madsen, J., 1994. Am. J. Physiol. 266, E357–E365.
Skjaervold, N.K., Aadahl, P., 2012. Acta Diabetol. 49, 489–491.
Sommer, J.R., Farley, R.T., Graham, K.R., Yang, Y., Xue, J., Reynolds, J.R., Schanze, K.S., 2009. ACS Appl. Mater. Interfaces 2, 274–278.
Steiner, M.-S., Duerkop, A., Wolfbeis, O.S., 2011. Chem. Soc. Rev. 40, 4805–4839.
Sternberg, E.D., Dolphin, D., Brückner, C., 1998. Tetrahedron 54, 4151–4202.
Thompson, R.B., 1994. In: Lakowicz, J.R. (Ed.), Topics in Fluorescence Spectroscopy. Plenum Press, New York.
Vinogradov, S.A., Wilson, D.F., 1995. J. Chem. Soc.: Perkin Trans. 2, 103–111.
Weinzimer, S., Xing, D., Tansey, M., Fiallo-Scharer, R., Mauras, N., Wysocki, T., Beck, R., Tamborlane, W., Ruedy, K., 2008. Diabetes Care 31, 525–527.
Weissleder, R., 2001. Nat. Biotechnol. 19, 316–317.
Wentholt, I.M.E., Maran, A., Masurel, N., Heine, R.J., Hoekstra, J.B.L., DeVries, J.H., 2007. Diabet. Med. 24, 527–532.
WHO, 2013. Diabetes Fact sheet No. 312. ⟨http://www.who.int/mediacentre/factsheets/fs312/en/⟩ (15.03.2014).
Xiang, H., Cheng, J., Ma, X., Zhou, X., Chruma, J.J., 2013. Chem. Soc. Rev. 42, 6128–6185.
Zajko, Š., Klimant, I., 2013. Sens. Actuators B: Chem. 177, 86–93.